







Article

Antibacterial Activity and Kinetic Release of *Laureliopsis philippiana* (Looser) Essential Oil from Nanostructured Porous Silicon with Surface-Functionalization Alternatives

Andrés Pérez-San Martín ¹, Karina Uribe ¹, Jacobo Hernández-Montelongo ^{2,*}, Nelson Naveas ^{3,4}, Miguel Manso-Silván ³, Patricio Oyarzún ⁵, Víctor Díaz-García ⁵, Braulio Contreras ⁵ and Gonzalo Recio-Sánchez ^{5,*}

- ¹ Department of Agricultural and Aquaculture Sciences, Universidad Católica de Temuco, Temuco 4813302, Chile
- ² Department of Physical and Mathematical Sciences, Faculty of Engineering, Universidad Católica de Temuco, Temuco 4813302, Chile
- ³ Departamento de Física Aplicada and Instituto de Ciencia de Materiales Nicolás Cabrera, Universidad Autónoma de Madrid, 28049 Madrid, Spain
- ⁴ Departamento de Ingeniería Química y Procesos de Minerales, Universidad de Antofagasta, Avenida Angamos 601, Antofagasta 1270300, Chile
- ⁵ Facultad de Ingeniería y Tecnología, Universidad San Sebastián, Lientur 1457, Concepcion 4080871, Chile
- * Correspondence: jacobohernandez@uct.cl (J.H.-M.); gonzalo.recio@uss.cl (G.R.-S.)



Citation: Pérez-San Martín, A.; Uribe, K.; Hernández-Montelongo, J.; Naveas, N.; Manso-Silván, M.; Oyarzún, P.; Díaz-García, V.; Contreras, B.; Recio-Sánchez, G. Antibacterial Activity and Kinetic Release of *Laureliopsis philippiana* (Looser) Essential Oil from Nanostructured Porous Silicon with Surface-Functionalization Alternatives. *Appl. Sci.* **2022**, *12*, 8258. <https://doi.org/10.3390/app12168258>

Academic Editor: Eric Guibal

Received: 6 July 2022

Accepted: 16 August 2022

Published: 19 August 2022

Publisher's Note: MDPI stays neutral with regard to jurisdictional claims in published maps and institutional affiliations.



Copyright: © 2022 by the authors. Licensee MDPI, Basel, Switzerland. This article is an open access article distributed under the terms and conditions of the Creative Commons Attribution (CC BY) license (<https://creativecommons.org/licenses/by/4.0/>).

Abstract: In this work, the antibacterial activity of *Laureliopsis philippiana* (Looser) essential oil was studied, and its kinetic release performance using different surface-functionalized nanostructured porous silicon (nPSi) was analyzed. Experimental results showed the high inhibitory effect of *Laureliopsis philippiana* essential oil against *Staphylococcus aureus* and *Klebsiella pneumoniae*. In addition, the essential oil was successfully loaded into different kinds of functionalized nPSi. FTIR measurements indicated the formation of stable complexes in the nPSi functionalization process. Specifically, chemical oxidized nPSi (nPSi-Ox), 3-aminopropyltriethoxysilane functionalized nPSi (nPSi-APTS), undecylenic acid-functionalized nPSi (nPSi-UAc), chitosan (nPSi-Chi) and β -cyclodextrin (nPSi- β CD) polymer functionalization on nPSi were studied. nPSi-Ox, nPSi-APTS, and nPSi-UAc were covalent functionalization, and nPSi-Chi and nPSi- β CD were obtained by electrostatic attachment. The kinetic study demonstrated a controlled release of up to 4 h for all the samples following a quasi-Fickian diffusion mechanism. Moreover, the use of functionalized nPSi-APTS and nPSi-UAc structures allows a more controlled kinetic release of *Laureliopsis philippiana* essential oil in comparison to the rest of the functionalization, increasing its availability and exposure to the environment.

Keywords: nanostructured porous silicon; surface functionalization; essential oil; *Laureliopsis philippiana*; antibacterial activity

1. Introduction

The use of natural products as a source of bioactive compounds has grown in recent years due to the extraction of secondary metabolites and their potential phytotherapeutic applications [1]. These extracts are typically characterized by the presence of alkaloids, flavonoids, terpenes, tannins, and/or phenols, which are heterogeneously distributed in whole plant systems. Furthermore, these components have been distinguished by their antioxidant, antimicrobial, antifungal, and antiviral activities against various pathogens and insects [2]. Therefore, they have been widely applied in the pharmaceutical, sanitary, agricultural, and food industries [3]. In this sense, essential oils are natural substances synthesized and stored in specialized secretory cells or plant organs, such as glandular

trichomes, resin ducts, or secretory cavities, and they play an important role in the protection and communication of plants with their environment [4]. These compounds are commonly extracted by hydrodistillation or steam distillation and consist of a complex mixture of monoterpenes, sesquiterpenes, and their derivatives, such as alcohol, aldehydes, esters, and ketones [4]. They are described as volatile, aromatic, oily, biologically active components with low toxicity and low environmental effects; thus, they are widely used in industry as an alternative to the excessive use of antibiotics [5,6].

Several studies have recently been reported focusing on describing the main composition of essential oils in aromatic worldwide species and studying their antibacterial and antifungal activities [7,8]. In the present work, we focus on an essential oil produced by the native species *Laureliopsis philippiana* (Looser) Schodde, which belongs to the Monimiaceae family and is mainly located in the forests of southern Chile and Argentina. This species has been traditionally used to treat headaches, colds, and nervous system disorders [9], and its antimicrobial and antifungal effects have recently been reported for bacteria of human interest, such as *Escherichia coli* and *Enterobacter* [10,11].

However, the high volatility of *Laureliopsis philippiana* essential oil affects its exposure to the environment, limiting its long-lasting bioavailability. Furthermore, its slight solubility and susceptibility to degradation in aqueous solutions caused by temperature, humidity, and light reduce its bioactivity. Moreover, oxidation of essential oils can produce radical reactive species [12]. In this context, the use of mesoporous nanomaterials aims to prevent rapid volatilization by enabling the controlled release of bioactive compounds [13]. Different kinds of mesoporous nanomaterials, including biodegradable biopolymer, silica nanoparticles, and hybrid nanomaterials, have successfully hosted volatile essential oils into nanoporous structures, demonstrating long-term antifungal and antibacterial activities [14–16]. For example, silica microcapsules allow the retention of fragrance release for up to 80 days [17]. Moreover, recent studies have reported advances in the surface modification of different structures to improve the release of volatile compounds with potential industrial use. Chemical and atmospheric-pressure plasma are some of the surface modification techniques that allow for the retention and release of essential oils [18,19]. In addition, functional biopolymers seem to be a potential option for improving the control release of volatile compounds [20].

In that sense, nanostructured porous silicon (nPSi), which can be obtained from electrochemical etching of silicon wafers in HF-based solutions, is one of the most promising nanomaterials for controlling the kinetic release of volatile compounds [21]. The mesoporous structure of nPSi can be easily tuned by controlling the main parameters of the fabrication process. In addition, its complex internal structure based on silicon nanocrystals embedded in an amorphous silicon matrix leads to high surface reactivity, which allows different kinds of functionalization processes [22]. Due to these properties, the controlled release of metallic nanoparticles, drugs, and volatile polyphenols has been investigated in recent years for biological and biomedical applications [23–25]. In the case of nPSi as a carrier of essential oils, no studies have been reported in the literature. However, some active compounds extracted from essential oils have been loaded into nPSi; for example, studies on the use of nPSi microparticles thermally oxidized for 1 h at 400 °C as a drug delivery system of trans-cinnamaldehyde, which is a molecule isolated from cinnamon essential oil [26]. Kinetic release is directly related to surface functionalization and depends on the kind of compound; the kinetic delivery of the target can be controlled [23]. In that sense, in this work, we studied for the first time the load and release of *Laureliopsis philippiana* (Looser) essential oil from different functionalized nPSi structures. The objective of this study is to evaluate the antibacterial activity of *Laureliopsis philippiana* (Looser) essential oil, and to analyze its kinetic release from different kinds of functionalized nPSi structures. In particular, nPSi mesoporous structures were chemically oxidized (nPSi-Ox), functionalized with 3-aminopropyltriethoxysilane (nPSi-APTS), undecylenic acid (nPSi-UAc), chitosan (nPSi-Chi) and β -cyclodextrin (nPSi- β CD).

2. Materials and Methods

2.1. Essential Oil Extraction

The essential oil was obtained from leaves of the species *Laureliopsis philippiana*, which were collected near Hornopirén, Hualaihué, in southern Chile (41°52'49.0" S, 72°26'31.5" W). Hydro-distillation was carried out using Clevenger-type equipment for 3 h, following the standard procedure of the European Pharmacopoeia reported by [27]. 100 g of dried ground plant material was added to a 1000 mL distillation balloon with distilled water and then boiled to 100 °C. The vapors were condensed on a cold surface (condenser), and the obtained essential oil was separated by the density difference. The recovered sample was dried with anhydrous sodium sulfate and filtered with a syringe (0.22 µm). Finally, the samples were stored under refrigeration at 5 °C in amber glass bottles.

2.2. Fabrication of Nanostructured Porous Silicon

2.2.1. Preparation and Oxidation of Nanostructured Porous Silicon

Nanostructured porous silicon (nPSi) layers were prepared by an electrochemical etching of p⁺ type silicon wafer (boron-doped, orientation <100>, resistivity = 0.001–0.005 Ω·cm) in HF:ethanol (1:2) solutions for 15 min at a current density of 60 mA/cm². Once the process was finished, the nPSi substrates were rinsed with ethanol and dried at room temperature. Straightaway, a chemical oxidation process (nPSi-Ox) was performed using H₂O₂ 50% v/v (150 vol.) as a solvent for 24 h at 20 °C in agitation at 50 rpm. Then, the samples were rinsed with ethanol, dried at room temperature, and stored.

2.2.2. Functionalization with Undecylenic Acid (nPSi-UAc)

Functionalization with fatty acids was performed using unoxidized nPSi plates immersed in 95% undecylenic acid. The plates were heated in a commercial consumer microwave oven at 280 W (60% potency) for 4 min and rinsed with hexane and twice with ethanol to remove excess.

2.2.3. Functionalization with 3-Aminopropyl-Triethoxysilane (nPSi-APTS)

The nPSi-Ox plates previously rinsed with ethanol were functionalized by immersing them for 15 min in 3-aminopropyl-triethoxysilane (APTS) 2% v/v in methanol under agitation at 50 rpm in the dark. The plates were then rinsed with ethanol and dried at room temperature. Finally, these were cured in a furnace at 120 °C for 20 min.

2.2.4. Functionalization with Chitosan (nPSi-Chi)

The nPSi-Ox plates were immersed in a chitosan solution 1% w/v for 10 min previously prepared with distilled water pH 4.0 and 570 µL acetic acid in agitation for 12 h, and adjusted to pH 4.0 with HCl and/or NaOH solution. Finally, the plates were rinsed with distilled water and dried at room temperature.

2.2.5. Functionalization with β-Cyclodextrin (nPSi-βCD)

Polymerization with β-cyclodextrin was performed using plates previously functionalized with chitosan in βCD solution for 15 min in agitation at 50 rpm. βCD solution was prepared with 10 g βCD, 3 g NaH₂PO₂ H₂O, and 10 g of citric acid in 100 mL of distilled water. Later, the plates were dried at room temperature and polymerized at 140 °C for 30 min. After cooling to room temperature, they were rinsed with distilled water and dried at 90 °C for 30 min.

2.3. Characterization Techniques

2.3.1. Gas Chromatography-Mass Spectrometry (GC-MS) Characterization

The essential oil was analyzed by GC/MS on a Shimadzu QP-2010 plus system equipped with an HP-5MS capillary column (30.0 m × 0.25 mm × 0.25 µm). The column temperature was maintained at 100 °C for 5 min for injection, then set at 20 °C/min to 200 °C and finally at 5 °C/min to 320 °C for 5 min. The sample injection (1 µL) was

performed in SPLIT ratio mode (1:10), and the injector temperature was maintained at 250 °C throughout the analysis (52 min). The carrier gas flow was operated in pressure control mode (14.3 kPa), with a column flow of 1.18 mL. The MS detector (electron impact ionization mode) was operated with an ion source and interface temperature of 260 °C using an ionization voltage of 70 eV in SIM mode for sample detection and quantification.

The components were identified by comparing their mass spectra with the NIST 08 and NIST 08s libraries. In addition, Kovats retention rates were calculated by LabSolutions v2.53 (GC/MS Solution Shimadzu; Kyoto, Japan) using an n-alkane standard C7–C30 (Supelco 49451-U), which was analyzed under the same chromatographic conditions as the sample and only considering the C10–C30 alkanes. Finally, the component concentration was obtained by semi-quantification using the relative area normalization method of the peaks and applying correction factors.

2.3.2. Antibacterial Evaluation

Staphylococcus aureus (Gram-positive) and *Klebsiella pneumoniae* (Gram-negative) cultures were incubated in LB medium at 37 °C by 24 h with *L. philippiana* essential oil and mineral oil in a concentration of 0, 0.1, 0.2, 0.3, 0.4, and 0.5 oil/LB medium volume ratios. The specific volume is reported in detail in the Supplementary Information (Table S1). The inhibition effects on bacterial growth were estimated by turbidity at an optical density of 600 nm using an Epoch microplate spectrophotometer (Biotek Instruments; Winooski, VT, USA).

2.3.3. Gravimetric Analysis

The porosity of the nPSi samples was obtained by gravimetric analysis according to the following equation:

$$\%P = \left(\frac{m_1 - m_2}{m_1 - m_3} \right) \times 100 \quad (1)$$

where m_1 is the mass of the Si wafer before electrochemical etching, m_2 is the mass of the sample just after anodization, and m_3 is the mass of the sample after rapid dissolution of the whole nPSi layer in a 3% KOH solution.

2.3.4. Scanning Electron Microscopy

The morphology of the samples was studied using field emission scanning electron microscopy (FE-SEM FEI VERIOS 460) operating with an acceleration potential of 2 keV.

2.3.5. IR Spectroscopy

Fourier-transformed infrared spectroscopy (FT-IR) was used for the chemical analyses of the nanostructures. FTIR spectra were carried out using an FT-IR spectrometer (CARY 630 FTIR Agilent Technologies, Santa Clara, CA, USA) in a range between 4000 and 600 cm^{-1} with a 1 cm^{-1} resolution (NS = 4).

2.3.6. Essential Oil Loading/Release Profiles

The functionalized nanostructures were loaded into a solution containing 750 μL of essential oil, 6 mL of dimethyl sulfoxide (DMSO), and 21 mL of phosphate-buffered saline (PBS). The plates were immersed in the solution under constant agitation at 50 rpm at a temperature of 25 °C for 24 h. After incubation, the plates were transferred to a PBS solution to evaluate the release concentration of each functionalization using UV-Vis spectroscopy. The essential oil was determined at a wavelength of 280 nm and measured at different time intervals. All experiments were conducted in triplicate. The same methodology was applied to control mineral oil.

To determine the mechanism of release, five models were fitted to the release profiles and described using the following equations:

Zero-order model:

$$F = K_0 \cdot t \quad (2)$$

where F is the fractional drug release, K_0 is the zero-order release constant, and t is the time release.

First-order model:

$$F = 100 \cdot (1 - e^{-K_1 \cdot t}) \quad (3)$$

where F is the fractional drug release at time t , and K_1 is the first-order release kinetic constant.

Korsmeyer–Peppas model:

$$F = K_{KP} \cdot t^n \quad (4)$$

where F is the fractional drug release, t is the release time, K_{KP} is the Korsmeyer–Peppas kinetic constant, and n is an exponent that characterizes the mechanism of drug release.

Higuchi model:

$$F = K_H \cdot t^{1/2} \quad (5)$$

where F is the fractional drug release at time t , and K_H is a Higuchi kinetic constant.

Hixson–Crowell model:

$$F = 100 \cdot [1 - (1 - K_{HC} \cdot t)^3] \quad (6)$$

where F is the fractional drug release at time t , and K_{HC} is the constant of incorporation, which relates surface and volume.

2.4. Data Analysis

Chemical structures were designed using ACD/ChemSketch (Freeware) v. 12.01 ©2010 software. The spectroscopic and fitting model analyses were carried out using OriginPro v8.0724 SR0 ©2007 software. Antibacterial activity was analyzed by comparison of means and post-hoc evaluation of significant differences by Kruskal–Wallis non-parametric analysis and Tukey HSD, respectively ($p < 0.05$).

3. Results and Discussion

3.1. Essential Oil Analysis

GC-MS analysis of *L. philipiana* essential oil showed the presence of 18 components (Table 1). The sample was characterized by a higher concentration of β -Linalool, β -Isosafrole, Eucalyptol, and Methyleugenol with 33.56, 17.39, 15.60, and 10.33% of abundance, respectively. The composition of the essential oil was similar to that previously reported in southern Chile [11]. The main differences found were the absence of the 3-Carene metabolite and the percentage concentration of the most abundant compounds. Some differences between the composition, quality, and quantity of extracted compounds may be due to diverse factors, such as climate, soil composition, plant organ, age, vegetative cycle stage, and analytical extraction methods.

Table 1. GC-MS chemical composition of the essential oil from *L. philipiana* leaves.

Compound	RT	Abundance (%)	KI ^a	KI ^b	Boiling Point (°C)
α -Pinene	5.6	1.74	948	931	156.2 ^c
β -Terpinene	6.5	1.67	993	971	173.5 ^c
β -Pinene	6.6	2.60	943	973	166.0 ^c
β -Myrcene	7.0	0.97	958	991	167.0 ^c
α -Phellandrene	7.3	6.17	969	1003	172.0 ^c
1, 3, 8- <i>p</i> -Menthatriene	7.8	0.56	1029	1023	195.0 ^d
Eucalyptol (1,8-Cineole)	8.0	15.6	1059	1029	176.4 ^c
Z- β -Ocimene	8.5	0.73	976	1048	177.0 ^d
Terpinolene	9.6	0.90	1052	1086	186.0 ^c
β -Linalool	10.0	33.56	1082	1103	197.5 ^c
Terpinen-4-ol	12.0	0.53	1137	1175	209.0 ^c

Table 1. Cont.

Compound	RT	Abundance (%)	KI ^a	KI ^b	Boiling Point (°C)
α -Terpineol	12.4	4.46	1143	1189	219.2 ^c
β -Isosafrole	15.1	17.39	1345	1288	253.0 ^c
Phenol, 2-methoxy-3-(2-propenyl)	16.9	0.61	1392	1356	286.4 ^e
Methyleugenol	18.2	10.33	1361	1405	262.6 ^c
Aromadendrene	18.5	0.52	1386	1416	257.0 ^d
α -Amorphene	20.0	0.58	1440	1478	303.2 ^e
γ -Elemene	20.4	1.08	1465	1494	258.0 ^d

RT = Retention time. ^a Kovats indices obtained from databases NIST08 and NIST08s. ^b Kovats indices are relative to the n-alkane (C7–C30) standard in a capillary column HP-5MS. ^c Data obtained from the National Center for Biotechnology Information (NCBI), PubChem database. ^d Data obtained from the Good Scents Company Information System (TGSC) database. ^e Data obtained from the Chemo database.

3.2. Antibacterial Activity

The antibacterial activity of *L. philippiana* essential oil was evaluated using *S. aureus* and *K. pneumoniae* strains. Figure 1 shows the experimental results of the antibacterial evaluation of the essential oil compared to the mineral oil. The latter was used as a control for traditionally lipophilic extracts to obtain essential oils, which could influence the antibacterial activity of the extract. Figure 1A shows a decrease in *S. aureus* viability over 90% and 15–70% of the essential oil and mineral oil, respectively. Data presented a statistically significant difference in all concentrations evaluated (0.1–0.5 Oil/medium ratio). On the other hand, *K. pneumoniae* strain viability (Figure 1B) reported decreasing viability values between 80–90% for the essential oil and between 25–70% for the mineral oil. In this case, only statistically significant differences were obtained in the concentrations 0.1, 0.2, and 0.3 Oil/medium ratio.

Antimicrobial testing demonstrated higher susceptibility in Gram-positive bacteria compared to Gram-negative bacteria. A similar behavior was previously reported for *L. philippiana* essential oil against Gram-negative (*E. aerogenes* and *E. coli*) and Gram-positive (*S. aureus* and *S. epidermidis*) strains [10], which was associated with small hydrophilic compounds such as oxygenated monoterpenes (linalool and eucalyptol) presented in the *L. philippiana* essential oil, which could be translated through the external membrane due to porin proteins which provide hydrophilic transmembrane channels [10]. Thus, the different susceptibility in Gram-positive and Gram-negative bacteria could be due to the complex outer rigid membrane of the latter, which is rich in lipopolysaccharide and limits the diffusion of the metabolites. In contrast, Gram-positive bacteria lack an extra complex membrane, increasing their susceptibility to small antimicrobial molecules. In turn, the infiltration of hydrophobic compounds is favored due to the lipophilic terminations present in the cell membrane, such as lipoteichoic acid [28]. Linalool may act as a protein-denaturing agent [28]. In addition, other compounds of *L. philippiana* essential oil can also contribute to antibacterial activity, including isosafrole, a Safrole isomer that has been reported to act as a precursor to Spathulenol, and methyleugenol, which has demonstrated antifungal effects against the phytopathogens *Alternaria* spp. and *Penicillium chrysogenum* [29,30].

It is also worth noting that the antimicrobial effect of *L. philippiana* essential oil remained unaffected while stored at 4 °C. The antimicrobial effect of the three-year-old extract stored at 4 °C is reported in the Supplementary Information (Figure S1). No significant differences were observed with respect to the antimicrobial effects of fresh oil.

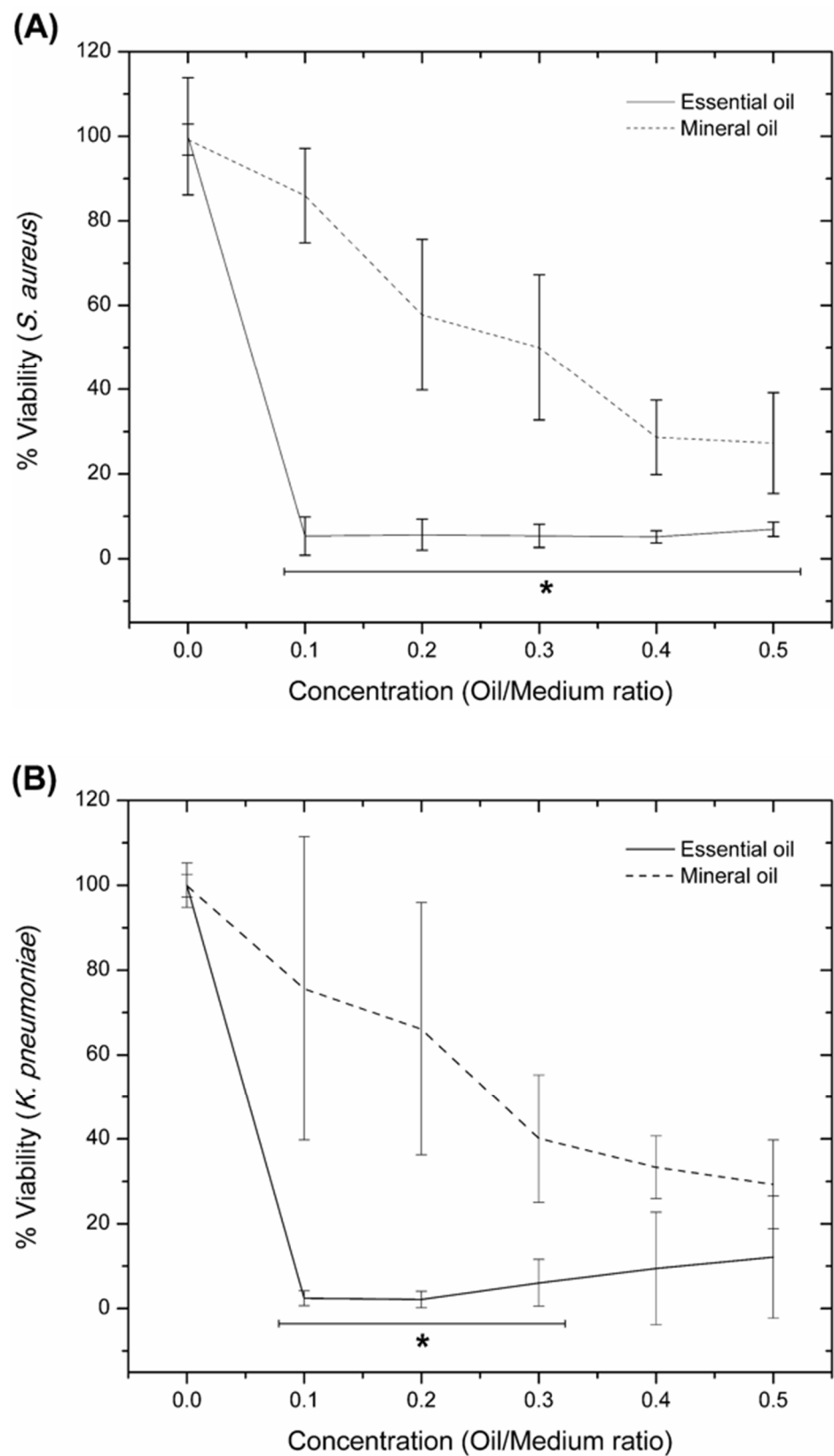


Figure 1. Bacterial growth inhibition in the presence of *L. philippiana* essential oil and mineral oil. The effect of different volume/volume ratio of essential oil (solid line) and mineral oil (segmented line) was evaluated using (A) *S. aureus* and (B) *K. pneumoniae*. Results were averaged from 3 independent experiments ($n = 3$). Statistically significant differences ($p < 0.05$) compared essential oil and mineral oil treatments are indicated with an asterisk (*).

3.3. Morphology of Nanostructured Porous Silicon

Field emission scanning electron microscopy (FE-SEM) was used to study the morphology of the nPSi structure. Figure 2A,B shows surface and cross-section images of a representative nPSi layer, respectively. The nPSi surface was characterized by a homogeneous pore distribution with a mean pore diameter of 14 ± 3 nm (Figure 2A). Moreover, as seen in Figure 2B, the thickness of the nPSi layer was $30 \mu\text{m}$ in depth, with a longitudinal column-like pore structure. On the other hand, the gravimetric analysis presented an average porosity of $75 \pm 5\%$ for this type of nPSi structure.

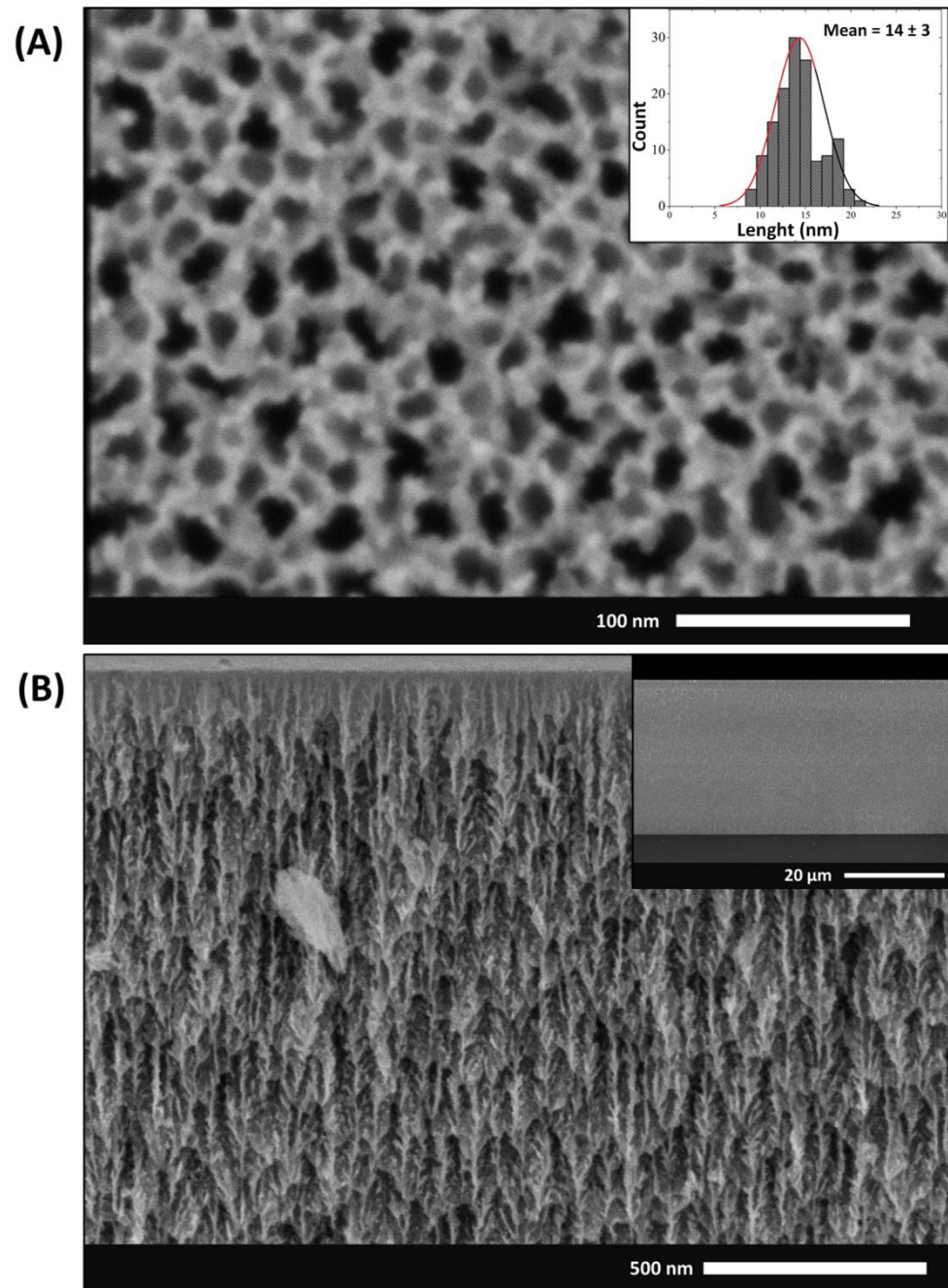


Figure 2. (A) FE-SEM image of the surface of the nPSi layer. Inset: distribution of pore size measurements. (B) Cross-section FE-SEM image of the nPSi layer. Inset: the same cross-section at lower magnification to see the total thickness of the thin film.

3.4. Surface Functionalization of Nanostructured Porous Silicon

The surface engineering of nPSi is an important step in using this material in biomedical applications, such as drug delivery carriers. Modifying the chemical surface of the nPSi structure allows the control of some parameters, including surface charge, hydrophilic behavior, and biocompatibility, which may have a considerable influence on managing essential oil load and release. Figure 3 depicts the reaction scheme for each surface functionalization of the nPSi layers studied in this work. By oxidizing the nPSi structure (nPSi-Ox), hydrophilic behavior is obtained, which enhances the loading of positively charged compounds and the degradation rate and allows further functionalization. Undecylenic acid functionalization increases the mechanical stability and solubility of nPSi (nPSi-UAc) due to the contribution of amphiphilic chains characterized by their apolar hydrocarbon chains and their polar acidic head. On the other hand, APTS (nPSi-APTS) and chitosan (nPSi-Chi) functionalization give a positive surface charge due to the amino groups, increasing the biocompatibility and load of negatively charged compounds. Finally, β -cyclodextrin polymerization (nPSi- β CD) enhances loading of insoluble compounds and controls kinetic release due to their cavity-like structure with a lipophilic cavity and hydrophilic surface.

To monitor the success of each process, FTIR measurements were carried out (Figure 4). The nPSi-Ox reaction was chemically induced by H_2O_2 . The FTIR spectrum shows a characteristic strong absorption band at 1040 cm^{-1} and a stretching mode shoulder at 1170 cm^{-1} , which are related to asymmetric stretching in Si-O from the Si-O-Si group, confirming the success of the process [22]. Additionally, weak absorbance bands appeared at 615 cm^{-1} and 790 cm^{-1} related to the Si-H and Si-OH bonds, respectively. Furthermore, a weak O-H stretching band from Si-OH groups appears at 3261 cm^{-1} and the surface signal assigned to $O_y\text{-Si-H}_x$ stretching mode can be observed at 885 cm^{-1} and 2100 cm^{-1} [22,23].

Undecylenic acid was grafted onto the nPSi layer according to the reaction shown in Figure 3B. During this process, the nPSi surface was hydrocarbonized. The FTIR spectrum demonstrated this state. Two absorption peaks were detected at 625 cm^{-1} and 2088 cm^{-1} corresponding to Si-H and Si-H_x groups stretching vibration and deformation mode, respectively. In addition, two absorption peaks appeared at 660 cm^{-1} and 912 cm^{-1} , related to Si-H₂ scissors bending and scissors mode [31]. On the other hand, the absence of a C=C band at 1645 cm^{-1} indicated the rupture of the double bond by union with a silicon surface [31]. An additional band is presented at 1713 cm^{-1} attributed to the C=O carboxyl group stretching vibration mode [32]. Furthermore, two additional bands were presented at 2855 and 2925 cm^{-1} described as the C-H stretching mode of an aliphatic chain [32].

3-aminopropyl-triethoxysilane was employed to functionalize the nPSi layers (nPSi-APTS) to incorporate amino groups on the surface (Figure 3C). The FTIR spectrum showed three different absorption bands at 3204 cm^{-1} , 1636 cm^{-1} , and 790 cm^{-1} caused by N-H stretching, and NH_2 bending, respectively. Moreover, two weak signals were observed at 2870 and 2938 cm^{-1} which could be assigned to the C-H bond due to asymmetrical and symmetrical stretching vibrations of CH_2 groups [33]. In addition, a strong band appears at 1035 cm^{-1} which may be attributed to the Si-O stretching band related to the Si-O-Si group formed between nPSi-Ox and APTS [33].

Chitosan was also utilized to functionalize the nPSi structure, and its chemical reaction is shown in Figure 3D. A strong absorption band appeared in the FTIR spectrum at 1040 cm^{-1} assigned to the Si-O-Si asymmetric stretching surface groups, demonstrating the absence of interactions with chitosan NH_3^+ groups [23]. Furthermore, two absorption peaks were observed at 790 cm^{-1} and 1636 cm^{-1} corresponding to the N-H stretching band and NH_3^+ symmetric deformation, respectively. Additionally, a weak peak emerges at 3321 cm^{-1} due to NH_2 stretching vibrations superposed on the wide band associated with the O-H groups [23].

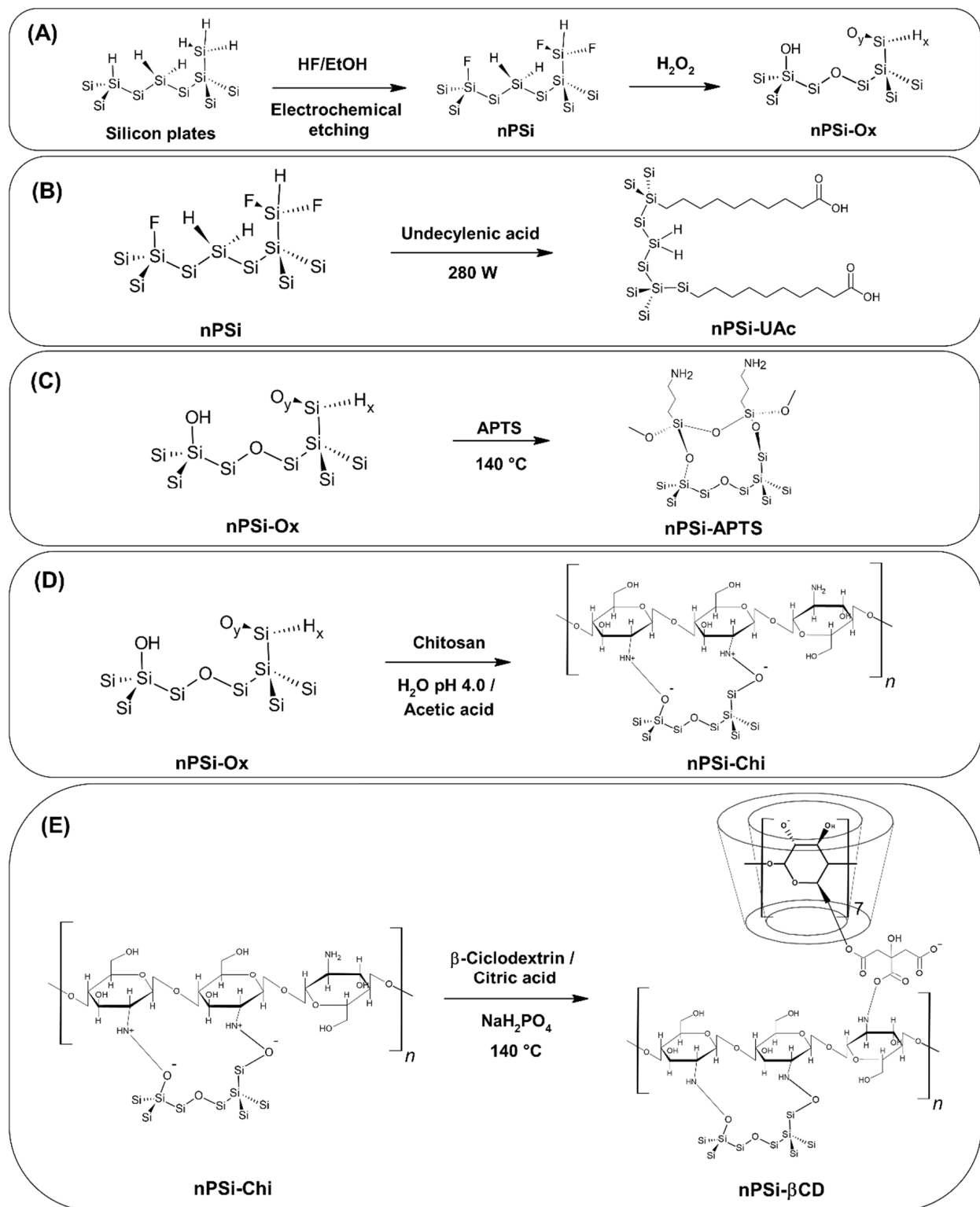


Figure 3. Nanostructured porous silicon (nPSi) synthesis and functionalization process. **(A)** nPSi synthesis and oxidation reaction (nPSi-Ox); **(B)** nPSi/Undecylenic acid reaction (nPSi-UAc); **(C)** nPSi-Ox/APTS reaction (nPSi-APTS); **(D)** nPSi-Ox Chitosan reaction (nPSi-Chi) and **(E)** nPSi-ox/ β CD reaction (nPSi- β CD).

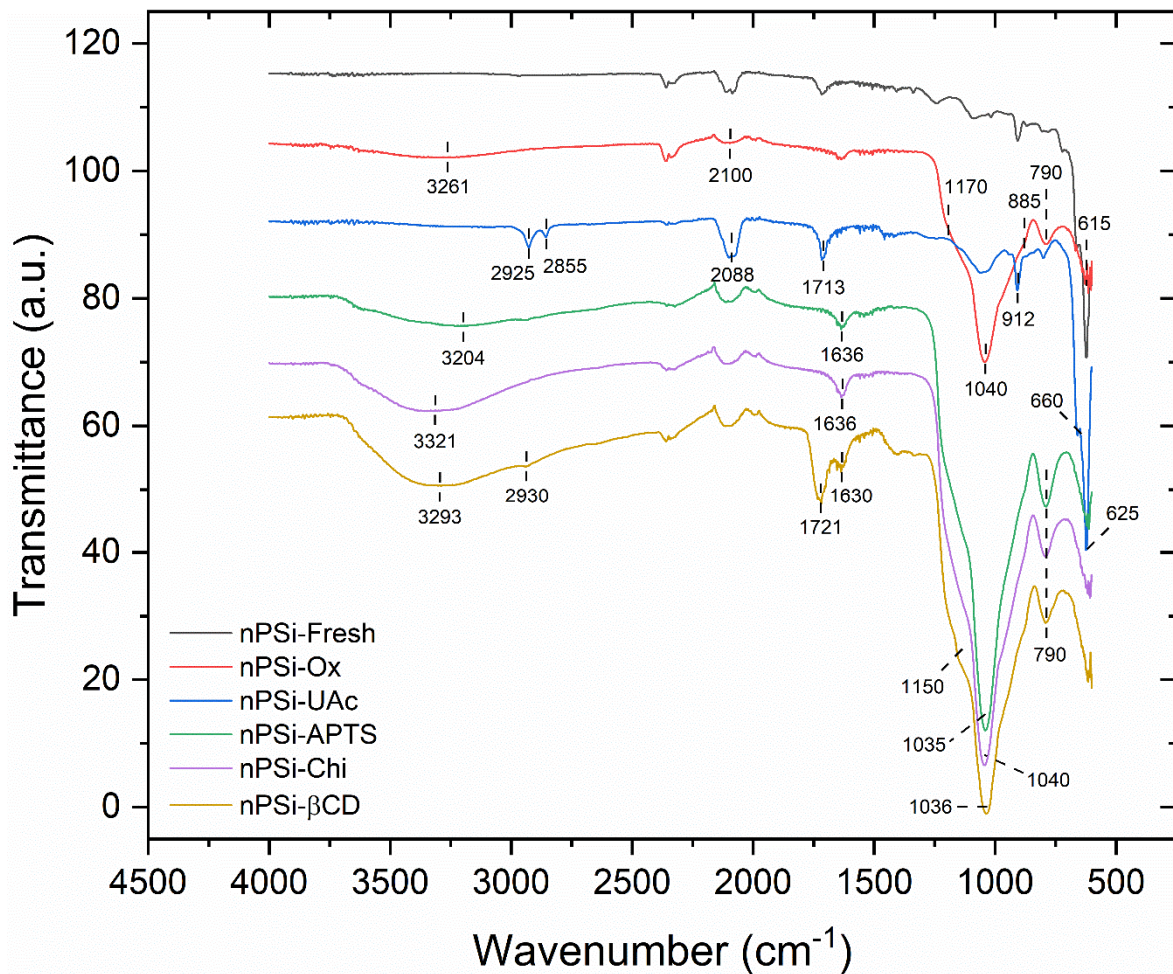


Figure 4. FT-IR spectra of the different functionalities of porous silicon nanostructures.

Finally, nPSi layers were also functionalized by a polymerization process using chitosan and β -cyclodextrin. The representation of the final structure is shown in Figure 3E. The FTIR spectrum presented a peak at 1721 cm^{-1} whose absorption was associated with the C=O stretching vibration of ester and carboxyl groups, which was attributed to the polymerization between β CD and citric acid [23]. In addition, strong absorption bands also appear at 1036 cm^{-1} and 1150 cm^{-1} , in this case attributed to C–OH stretching vibration and C–O–C stretching, respectively [23]. Moreover, a band located at 2930 cm^{-1} was described as CH_2 asymmetric stretching vibration band, and the one found at 3293 cm^{-1} was associated with O–H stretching groups [23]. The absorption peak located at a shorter wavenumber (790 cm^{-1}) is associated with N–H stretching band vibration, as in the nPSi-Chi sample, since this stage is preliminar to the synthesis of nPSi- β CD. Finally, the peak observed at 1630 cm^{-1} could represent the molecular water (H_2O) deformation bands [34].

Hence, these results indicate that the chemical engineering functionalization processes to obtain each nPSi structure with different surface chemistry were successful.

3.5. Kinetic and Release Models

Figure 5 shows the experimental release profiles of the essential oil obtained for each functionalization. The models were evaluated up to 4 h, the moment at which a constant cumulative release of essential oil into the solution was observed. In that sense, the controlled release reached a maximum at time of 0.5 h for nPSi-Chi (Figure 5D), 2 h for the cases of nPSi-Ox, nPSi-UAc and nPSi- β CD (Figure 5A,B,E, respectively), and 4 h for nPSi-APTS (Figure 5C). Variations in the release profiles were due to the volatile

chemical compounds from *L. philippiana* essential oil, which easily evaporated at normal temperatures.

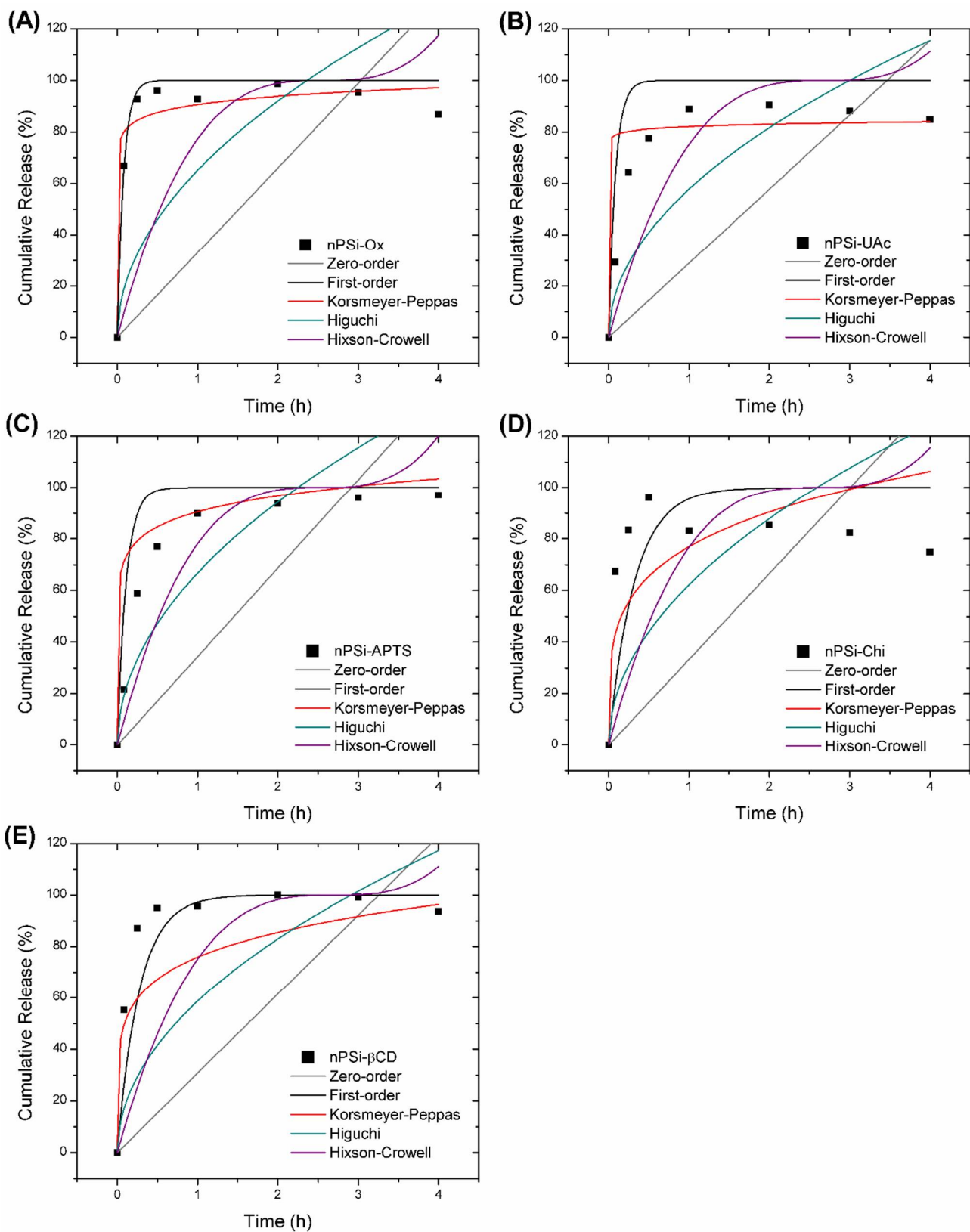


Figure 5. Essential oil kinetic release profile with different functionalities of nanostructured porous silicon. (A) nPSi-Ox, (B) nPSi-UAc, (C) nPSi-APTS, (D) nPSi-Chi, and (E) nPSi-βCD.

Moreover, to understand the release mechanism of each functionalization, kinetic profiles were fitted to five different models, including the Zero-order, First-order, Korsmeyer–Peppas, Higuchi, and Hixson–Crowell models, whose data are summarized in Table 2. All samples except for nPSi-Chi presented better adjustment with the First-order model, where the immediate-release dosage was dispersed in a single action [21]. In the case of nPSi-Chi, the essential oil release kinetics were more accurately described using the Korsmeyer–Peppas model. This result suggests that the governing factor of essential oil release could be attributed to the Fickian diffusion process [21,23].

Table 2. Essential oil kinetic release models using different functionalizations of nPSi.

Sample	Zero-Order		First-Order		Korsmeyer–Peppas			Higuchi		Hixson–Crowell	
	$R^2_{adj.}$	K_0	$R^2_{adj.}$	K_1	$R^2_{adj.}$	K_{KP}	n	$R^2_{adj.}$	K_H	$R^2_{adj.}$	K_{HC}
nPSi-Ox	−2.1228	33.01	0.9650	12.83	0.9329	90.66	0.050	−0.4705	65.08	0.4441	0.39
nPSi-UAc	−0.7239	30.72	0.9237	3.59	0.8699	75.77	0.173	0.3759	58.61	0.4859	0.37
nPSi-APTS	−0.2184	33.27	0.9875	3.11	0.8944	76.91	0.233	0.6330	62.12	0.7253	0.38
nPSi-Chi	−2.4854	28.87	0.7481	11.75	0.9156	82.10	0.016	−0.7720	57.75	−0.7630	0.37
nPSi-βCD	−1.5574	34.35	0.9897	9.07	0.9225	90.49	0.096	−0.0869	66.72	−0.0515	0.40

$R^2_{adj.}$ = regression coefficient adjusted; K_0 = Zero-order release rate constant (h^{-1}); K_1 = First-order release rate constant (h^{-1}); K_{KP} = Korsmeyer–Peppas release rate constant (h^{-n}); n = drug release exponent; K_H = Higuchi rate constant ($h^{-1/2}$) and K_{HC} = cube root law release constant ($h^{-1/3}$).

However, as the obtained $R^2_{adj.}$ values obtained by the First-Order and Korsmeyer–Peppas models are similar, the Akaike Information Criterion (AIC) was applied to determine a preferential model. This fined technique is based on in-sample fitting to estimate the likelihood of a model and predict future values. The best model is one that has a smaller AIC parameter [35]. These results showed that the essential oil kinetic release did not present significant differences among the samples determined by the F-test (Table 3). This parameter is used when comparing statistical models that have been fitted using the same underlying factors and data, and as a complement to the AIC parameter [36]. Only the nPSi-Chi samples showed significant differences, which is better described by the Korsmeyer–Peppas model. Therefore, according to the AIC results, both models, First-Order and Korsmeyer–Peppas, could accurately describe the release of *Laureliopsis philippiana* essential oil from nPSi structures. In this sense, the parameters of both models were analyzed. The First-order release kinetic constant (K_1) was associated with the release rate. K_1 values of the samples were nPSi-Ox > nPSi-Chi > nPSi-βCD > nPSi-UAc > nPSi-APTS, which indicated that the oxidized samples showed the fastest release profile, and nPSi-UAc and nPSi-APTS presented the most controlled release. Analyzing the Korsmeyer–Peppas release kinetic constant (K_{KP}), values presented a similar tendency: nPSi-Ox > nPSi-βCD > nPSi-Chi > nPSi-APTS > nPSi-UAc, suggesting that essential oil release was faster on oxidized samples and more controlled on nPSi-APTS and nPSi-UAc structures. Finally, concerning the release exponent n of the Korsmeyer–Peppas model, which determines the mechanism of diffusion, all samples presented a smaller value than 0.5. These values suggest that a quasi-Fickian diffusion mechanism governed the release of essential oil from all nPSi samples [21,23,37].

These results could be explained by the complex composition of *Laureliopsis philippiana* essential oil, which involves diverse organic and aromatic molecules. These structures are characterized by low molecular weight volatile hydrocarbons. Among them, the presence of β-Linalool (33.56%), β-Isosafrole (17.39%), eucalyptol (15.6%), and methyleugenol (10.33%) was highlighted. According to the chemical structure of these molecules (Figure 6), the main interactions with functionalized samples (Figure 3) could be electrostatic interactions and Van der Waals forces. These compounds presented poor interaction with the oxidized surface of nPSi-Ox, which justifies the fast step-like release profile observed and denotes poor temporal regulation of the release with those structures. A similar behavior was observed for nPSi-βCD samples. However, the compatible hydrocarbonized surface of the

nPSi-UAc sample could interact more effectively via hydrogen bonds with these volatile compounds, thus controlling the kinetic release of the essential oil. Likewise, it is suggested that amino groups present on the nPSi-APTS surface could also interact electrostatically due to the amine groups of APTS to control the release profile of the essential oil. In the case of nPSi-Chi, which also presents amine groups, it is important to mention that this functionalization was weaker by adsorption and that APTS was covalently. This could also explain the higher variations in release profiles. Overall, this experimental strategy has the potential to control the volatility of *Laureliopsis philippiana* essential oil on the road to develop long-term antibacterial applications.

Table 3. Model comparison by AIC and F-Value.

Sample	Akaike Information Criterion (AIC)		F-Value
	First-Order	Korsmeyer-Peppas	
nPSi-Ox	34.62239	44.19362	ns
nPSi-UAc	40.89699	49.53074	ns
nPSi-APTS	28.16102	49.58153	ns
nPSi-Chi	48.77567	44.39639	14.89 *
nPSi- β CD	25.50497	46.01561	ns

(*) $p < 0.05$; (ns) no significant.

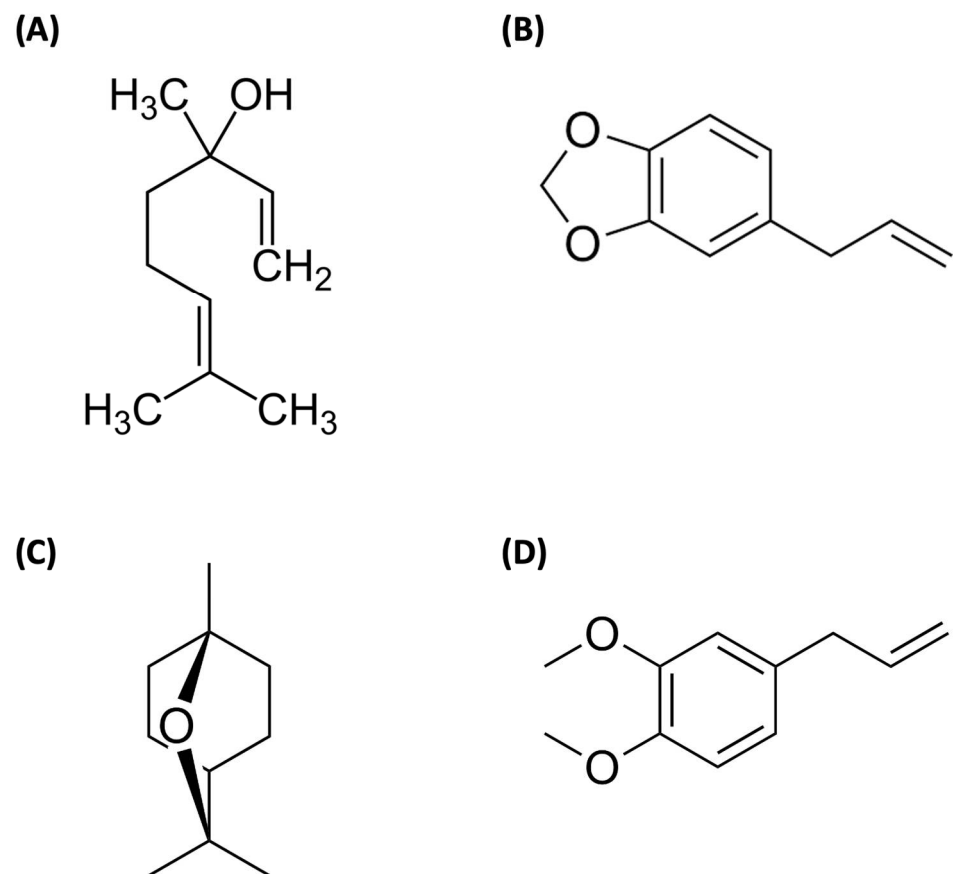


Figure 6. Chemical structure of the most abundant compounds in *Laureliopsis philippiana* essential oil: β -Linalool (A), β -Isosafrole (B), Eucalyptol (1,8-Cineole) (C) and Methyleugenol (D).

4. Conclusions

Laureliopsis philippiana essential oil was chemically characterized, and its main components were β -Linalool, β -Isosafrole, Eucalyptol, and Methyleugenol. In addition, it showed high inhibitory antibacterial activity against Gram-positive *S. aureus* and Gram-negative

K. pneumonia in comparison to mineral oil. The chemical functionalization of nPSi was demonstrated as an effective alternative to allow loading and controlled kinetic release of *L. philippiana* essential oil. The presence of different degrees of interaction of the essential oil components with the nPSi structures was demonstrated by the loading/release of the essential oil over time. The release profiles were studied for up to 4 h. According to the kinetics data, the diffusive mechanism of essential oil release was better explained by the First-order and Korsmeyer–Peppas models, suggesting a quasi-Fickian diffusion mechanism. Between all functionalizations studied in this work, nPSi-APTS and nPSi-UAc presented the best controlled release due to the interaction of the substrate with the essential oil. Finally, these results could indicate that *L. philippiana* essential oil may increase its sustained release time into the environment through the use of functionalized nPSi structures, which is interesting due to the scarce reports about it and its potential applications in the biomedical sector.

Supplementary Materials: The following supporting information can be downloaded at: <https://www.mdpi.com/article/10.3390/app12168258/s1>, Figure S1. Comparison of bacterial growth inhibition of essential oil in different years. The effect of different volume/volume ratio of essential oil (solid line) and three-year-old essential oil (segmented line) was evaluated using (A) *Staphylococcus aureus* and (B) *Klebsiella pneumoniae*. The essential oil three-year-old result was from 1 independent experiment ($n = 1$). Table S1. Incubation protocol for the antibacterial evaluation of *L. philippiana* essential oil and mineral oil.

Author Contributions: Conceptualization, G.R.-S., A.P.-S.M. and K.U.; porous silicon synthesis, A.P.-S.M. and K.U.; porous silicon functionalization, A.P.-S.M., K.U. and J.H.-M.; physicochemical characterizations, K.U., N.N. and M.M.-S.; release profiles, A.P.-S.M. and K.U.; mathematical analysis, A.P.-S.M. and J.H.-M.; biological characterizations, P.O., V.D.-G. and B.C.; writing—original draft preparation, G.R.-S., A.P.-S.M. and K.U.; project administration, G.R.-S. All authors have read and agreed to the published version of the manuscript.

Funding: This research was funded by the National Agency for Research and Development (ANID) of Chile through the grants DOCTORADO NACIONAL/2020—21201805, CONICYT PFCHA/DOCTORADO/2017-21172001, and FONDECYT POSTDOCTORADO 3190734.

Institutional Review Board Statement: Not applicable.

Informed Consent Statement: Not applicable.

Data Availability Statement: The data that support the findings of this study are available from the corresponding author upon reasonable request.

Acknowledgments: Andrés Pérez-San Martín thanks Ph.D. Program “Ciencias Agropecuarias” from Universidad Católica de Temuco. Nelson Naveas thanks Ph.D. Programs in “Advanced Materials and Nanotechnologies” from Universidad Autónoma de Madrid (UAM, Spain) and “Ingeniería de Procesos de Minerales” from Universidad de Antofagasta (UA, Chile).

Conflicts of Interest: The authors declare no conflict of interest.

References

1. Chukwuma, C.I.; Matsabisa, M.G.; Ibrahim, M.A.; Erukainure, O.L.; Chabalala, M.H.; Islam, M.S. Medicinal plants with concomitant anti-diabetic and anti-hypertensive effects as potential sources of dual acting therapies against diabetes and hypertension: A review. *J. Ethnopharmacol.* **2019**, *235*, 329–360. [[CrossRef](#)]
2. Lu, J.; Fu, X.; Liu, T.; Zheng, Y.; Chen, J.; Luo, F. Phenolic composition, antioxidant, antibacterial and anti-inflammatory activities of leaf and stem extracts from *Cryptotaenia japonica* Hassk. *Ind. Crops Prod.* **2018**, *122*, 522–532. [[CrossRef](#)]
3. Anand, U.; Jacobo-Herrera, N.; Altemimi, A.; Lakhssassi, N. A Comprehensive Review on Medicinal Plants as Antimicrobial Therapeutics: Potential Avenues of Biocompatible Drug Discovery. *Metabolites* **2019**, *9*, 258. [[CrossRef](#)]
4. Aziz, Z.A.; Ahmad, A.; Setapar, S.H.M.; Karakucuk, A.; Azim, M.M.; Lokhat, D.; Rafatullah, M.; Ganash, M.; Kamal, M.A.; Ashraf, G.M. Essential Oils: Extraction Techniques, Pharmaceutical and Therapeutic Potential—A Review. *Curr. Drug Metab.* **2018**, *19*, 1100–1110. [[CrossRef](#)]
5. Baptista-Silva, S.; Borges, S.; Ramos, O.L.; Pintado, M.; Sarmiento, B.J. The progress of essential oils as potential therapeutic agents: A review. *Essent. Oil Res.* **2020**, *32*, 279–295. [[CrossRef](#)]

6. Jugreet, B.S.; Mahomoodally, M.F.; Sinan, K.I.; Zengin, G.; Abdallah, H.H. Chemical variability, pharmacological potential, multivariate and molecular docking analyses of essential oils obtained from four medicinal plants. *Ind. Crops Prod.* **2020**, *150*, 112394. [CrossRef]
7. Reyes-Jurado, F.; Navarro-Cruz, A.R.; Ochoa-Velasco, C.E.; Palou, E.; López-Malo, A.; Ávila-Sosa, R. Essential oils in vapor phase as alternative antimicrobials: A review. *Crit. Rev. Food Sci. Nutr.* **2020**, *60*, 1641–1650. [CrossRef]
8. Raveau, R.; Fontaine, J.; Lounès-Hadj Sahraoui, A. Essential Oils as Potential Alternative Biocontrol Products against Plant Pathogens and Weeds: A Review. *Foods* **2020**, *9*, 365. [CrossRef]
9. Molares, S.; Ladio, A. Ethnobotanical review of the Mapuche medicinal flora: Use patterns on a regional scale. *J. Ethnopharmacol.* **2009**, *122*, 251–260. [CrossRef]
10. Toledo, D.; Mutis, A.; Hormazabal, E.; Quiroz, A.; Palma, R.; Parada, M.; Scheuermann, E. Chemical composition and antibacterial activity of *Laureliopsis philippiana* (Looser) essential oil. *Boletín Latinoam. Caribe Plantas Med. Aromáticas* **2014**, *13*, 117–125. Available online: <https://www.redalyc.org/articulo.oa?id=85629766012> (accessed on 5 July 2022).
11. Norambuena, C.; Silva, G.; Urbina, A.; Figueroa, I.; Rodríguez-Maciel, J.C. Insecticidal activity of *Laureliopsis philippiana* (Looser) Schodde (Atherospermataceae) essential oil against *Sitophilus* spp. (Coleoptera Curculionidae). *Chil. J. Agric. Res.* **2016**, *76*, 330–336. [CrossRef]
12. Alfei, S.; Oliveri, P.; Malegori, C. Assessment of the Efficiency of a Nanospherical Gallic Acid Dendrimer for Long-Term Preservation of Essential Oils: An Integrated Chemometric-Assisted FTIR Study. *ChemistrySelect* **2019**, *4*, 8891–8901. [CrossRef]
13. Vurro, M.; Miguel-Rojas, C.; Pérez-de-Luque, A. Safe nanotechnologies for increasing the effectiveness of environmentally friendly natural agrochemicals. *Pest Manag. Sci.* **2019**, *75*, 2403–2412. [CrossRef]
14. Liu, X.; Jia, J.; Duan, S.; Zhou, X.; Xiang, A.; Lian, Z.; Ge, F. Zein/MCM-41 Nanocomposite Film Incorporated with Cinnamon Essential Oil Loaded by Modified Supercritical CO₂ Impregnation for Long-Term Antibacterial Packaging. *Pharmaceutics* **2020**, *12*, 169. [CrossRef]
15. Chen, H.; Shen, Z.; Wu, P.; Zhou, H.; Hao, L.; Xu, H.; Zhou, X. Long effective tea tree oil/mesoporous silica sustained release system decorated by polyethyleneimine with high antibacterial performance. *J. Dispers. Sci. Technol.* **2020**, *42*, 1448–1459. [CrossRef]
16. Sattary, M.; Amini, J.; Hallaj, R. Antifungal activity of the lemongrass and clove oil encapsulated in mesoporous silica nanoparticles against wheat's take-all disease. *Pestic. Biochem. Phys.* **2020**, *170*, 104696. [CrossRef]
17. Yeom, J.; Shim, W.S.; Kang, N.G. Eco-Friendly Silica Microcapsules with Improved Fragrance Retention. *Appl. Sci.* **2022**, *12*, 6759. [CrossRef]
18. Gagliano Candela, R.; Maggi, F.; Lazzara, G.; Rosselli, S.; Bruno, M. The Essential Oil of *Thymbra capitata* and its Application as a Biocide on Stone and Derived Surfaces. *Plants* **2019**, *8*, 300. [CrossRef]
19. Boonmee, T.; Wongthaveethong, L.; Sinpoo, C.; Disayathanoowat, T.; Pettis, J.S.; Chaimanee, V. Surface Modification of Materials by Atmospheric-Pressure Plasma to Improve Impregnation with Essential Oils for the Control of *Tropilaelaps* Mites in Honeybees (*Apis mellifera*). *Appl. Sci.* **2022**, *12*, 5800. [CrossRef]
20. Biddeci, G.; Cavallaro, G.; Di Blasi, F.; Lazzara, G.; Massaro, M.; Milioto, S.; Parisi, F.; Riela, S.; Spinelli, G. Halloysite nanotubes loaded with peppermint essential oil as filler for functional biopolymer film. *Carbohydr. Polym.* **2016**, *152*, 548–557. [CrossRef]
21. Guzmán-Oyarzo, D.; Plaza, T.; Recio-Sánchez, G.; Abdalla, D.; Salazar, L.A.; Hernández-Montelongo, J. Use of nPSi-βCD Composite Microparticles for the Controlled Release of Caffeic Acid and Pinocembrin, Two Main Polyphenolic Compounds Found in a Chilean Propolis. *Pharmaceutics* **2019**, *11*, 289. [CrossRef]
22. Rodríguez, C.; Muñoz Noval, A.; Torres-Costa, V.; Ceccone, G.; Manso Silván, M. Visible Light Assisted Organosilane Assembly on Mesoporous Silicon Films and Particles. *Materials* **2019**, *12*, 131. [CrossRef]
23. Hernández-Montelongo, J.; Oria, L.; Cárdenas, A.B.; Benito, N.; Romero-Sáez, M.; Recio-Sánchez, G. Nanoporous Silicon Composite as Potential System for Sustained Delivery of Florfenicol Drug. *Phys. Status Solidi B Basic Res.* **2018**, *255*, 1700626. [CrossRef]
24. Le, N.T.; Kalluri, J.R.; Loni, A.; Canham, L.T.; Coffey, J.L. Biogenic Nanostructured Porous Silicon as a Carrier for Stabilization and Delivery of Natural Therapeutic Species. *Mol. Pharm.* **2020**, *14*, 4509–4514. [CrossRef]
25. Hernández-Montelongo, J.; Fernández-Fierro, C.; Benito-Gómez, N.; Romero-Sáez, M.; Parodi, J.; Carmona, E.R.; Recio-Sánchez, G. Hybrid porous silicon/green synthesized Ag microparticles as potential carriers for Ag nanoparticles and drug delivery. *Mater. Sci. Eng. C* **2020**, *116*, 111183. [CrossRef]
26. Jailani, A.; Kalimuthu, S.; Rajasekar, V.; Ghosh, S.; Collart-Dutilleul, P.-Y.; Fatima, N.; Koo, H.; Solomon, A.P.; Cuisinier, F.; Neelakantan, P. *Trans*-Cinnamaldehyde Eluting Porous Silicon Microparticles Mitigate Cariogenic Biofilms. *Pharmaceutics* **2022**, *14*, 1428. [CrossRef]
27. Bouin, A.S.; Wierer, M. Quality standards of the European Pharmacopoeia. *J. Ethnopharmacol.* **2014**, *158*, 454–457. [CrossRef]
28. Hyldgaard, M.; Mygind, T.; Meyer, R.L. Essential oils in food preservation: Mode of action, synergies, and interactions with food matrix components. *Front. Microbiol.* **2012**, *3*, 12. [CrossRef]
29. Stefan, M.; Zamfirache, M.; Padurariu, C.; Truta, E.; Gostin, I. The composition and antibacterial activity of essential oils in three *Ocimum* species growing in Romania. *Cent. Eur. J. Biol.* **2013**, *8*, 600–608. [CrossRef]

30. Madrid, A.; Godoy, P.; González, S.; Zaror, L.; Moller, A.; Werner, E.; Cuellar, M.; Villena, J.; Montenegro, I. Chemical Characterization and Anti-Oomycete Activity of *Laureliopsis philippianna* Essential Oils against *Saprolegnia parasitica* and *S. australis*. *Molecules* **2015**, *20*, 8033–8047. [[CrossRef](#)]
31. Oliinyk, B.V.; Lysenko, V.; Alekseev, S. Determining the impact of hydrofluoric acid on surface states of as-prepared and chemically modified Si nanocrystals. *RSC Adv.* **2016**, *6*, 3723–3728. [[CrossRef](#)]
32. Schiattarella, C.; Terracciano, M.; Defforge, T.; Gautier, G.; Ventura, D.; Moretta, R.; De Stefano, L.; Velotta, R.; Rea, I. Photoemissive properties and stability of undecylenic acid-modified porous silicon nanoparticles in physiological medium. *Appl. Phys. Lett.* **2019**, *114*, 113701. [[CrossRef](#)]
33. Azarshin, S.; Moghadasi, J. Surface functionalization of silica nanoparticles to improve the performance of water flooding in oil wet reservoirs. *Energy Explor. Exploit.* **2017**, *35*, 685–697. [[CrossRef](#)]
34. Rachmawati, H.; Edityaningrum, C.A.; Mauludin, R. Molecular Inclusion Complex of Curcumin- β -Cyclodextrin Nanoparticle to Enhance Curcumin Skin Permeability from Hydrophilic Matrix Gel. *AAPS PharmSciTech* **2013**, *14*, 1303–1312. [[CrossRef](#)]
35. Mohammed, A.A.; Naugler, C.; Far, B.H. Chapter 32—Emerging business intelligence framework for a clinical laboratory through big data analytics. *Emerg. Trends Comput. Biol. Bioinform. Syst. Biol.* **2015**, 577–602. [[CrossRef](#)]
36. Kissell, R.; Poserina, J. Chapter 2 Regression Models. *Optim. Sports Math Stat. Fantasy* **2017**, 39–67. [[CrossRef](#)]
37. Shetta, A.; Kegere, J.; Mamdouh, W. Comparative study of encapsulated peppermint and green tea essential oils in chitosan nanoparticles: Encapsulation, thermal stability, in-vitro release, antioxidant and antibacterial activities. *Int. J. Biol. Macromol.* **2019**, *126*, 731–742. [[CrossRef](#)]